On-line quantification of solid-phase metal extraction efficiencies using instrumented millifluidics platform

Fabien L. Olivier, Sarah M. Chevrier, Barbara Keller, Jean-Christophe Gabriel

On-line Quantification of Solid-Phase Metal Extraction Efficiencies Using Instrumented Millifluidics Platform

Fabien L. Olivier,[1, 2] Sarah M. Chevrier,[1, 2] Barbara Keller,[3] and Jean-Christophe P. Gabriel[1, 2] *

[1] Université Paris-Saclay, CEA, CNRS, NIMBE, LICSEN, F-91191, Gif-Sur-Yvette, France

[2] SCARCE Laboratory, Energy Research Institute @ NTU (ERI@N), Nanyang Technological University, 637553, Singapore

[3] Université Grenoble Alpes, CEA, IRIG-MEM, F-38054 Grenoble, FranceCorresponding author: JCP Gabriel, jean-christophe.gabriel@cea.fr

ABSTRACT: A semi-automated and fully integrated millifluidic platform has been developed for rapid development and study of Solid-phase extraction (SPE) processes. In this instrumented setup, the fluid coming out of the extraction mini-column is analysed directly using on-line X-ray fluorescence, enabling a real-time, fast and accurate measurement of the elemental concentrations within the flowing liquid. This platform aims at enhancing and facilitating the development of SPEs whose numerous experimental parameters make it time consuming to optimize and upscale. Hence, this approach solves the labour intensity issue and is as accurate as off-line Inductively Coupled Plasma, for instance. This is exemplified with a system comprising of a mixture of Rare-Earth Elements (REEs) and Iron, whose separation is investigated as a function of various experimental parameters. It enabled us to study the performance of the newly released METALICAPT® commercial materials and to determine an optimized path towards the almost total separation of Iron from the initial mixture. Overall, the original SPE process reported herein demonstrates the platform's reliability, performance and range of applicability.

Keywords: Solid-phase Extraction, Adsorption, Rare-Earth Elements, X-ray Fluorescence, Cation-exchange fiber

1. Introduction

Solid-phase-extraction (SPE) belongs to the world of chromatography and consists of eluting a mobile – liquid – phase containing dissolved species through to a stationary – solid – phase. The aim of such a process is to remove one or more compounds from the continuous - liquid - phase by taking advantage of their affinity towards the solid they are in contact with. SPE processes are mainly implemented for chemical, pharmaceutical, food or cosmetic purposes [1–3]. Well-known processes based on SPE, such as High-Performance Liquid Chromatography (HPLC), aim at highly purifying solutions by removing unwanted impurities. However, one of the drawbacks of SPE lies in the solid-phase, which is the most expensive part of the process, as it needs to be renewed regularly because its efficiency decreases from one extraction cycle to another. This, added to the considerable time needed to develop a process, deters efforts to optimize SPE.

The metal SPE processes considered in this report are based on a three step cycle. Each step is followed by an intermediate wash using a neutral liquid solution (usually deionized (DI) water), which removes the previously eluted solution from the solid phase enclosure. The first step of a cycle is the elution of the liquid phase to be purified, where species are interacting with the solid phase. This step is then followed by the desorption of the captured compounds and finally, the last step of the cycle, which enables a regeneration of the solid phase for the next cycle. Consequently, one may foresee that many parameters must be taken into account when implementing and optimizing such a process [4]: flowrates of the solutions to be eluted, desorption solution, regeneration solution, etc. Finding the optimal parameters for a given SPE is a long-standing effort, which requires non-negligible upstream studies. This is of particular interest when dealing with metal recycling SPE processes involving Rare-Earth Elements (REEs) and Iron. Indeed, lots of work has been done in the past few years focusing on the recovery of the elements commonly found in magnets, e.g. Neodymium-Iron-Boron magnets (NdFeB) [5–12] or electronic components that can be enriched in REEs, such as Nd-based capacitors [13].

Most of these previous studies deal with SPEs followed by time consuming and/or expensive off-line analysis of their output, using either Inductively Coupled Plasma by Optical Emission Spectroscopy (ICP-OES) [14], X-Ray Fluorescence (XRF) [15] or liquid chromatography coupled with Mass Spectrometry (MS) [16,17]. The drawbacks of these off-line measurements are that they: (i) require a larger sample size; (ii) may need further sample preparation and; (iii) may destroy the sample.

Hence the present study, which reports the first semi-automatized and fully integrated millifluidic platform performing SPE processes and enabling real-time metallic concentration measurement using an on-line XRF analysis. We will present the XRF integrated millifluidics platform in detail, as well as its usage, performance and interest. To illustrate its performance, we choose the application case of the SPE of Lanthanum, Neodymium, Ytterbium and their separation from Iron. We will show that the platform allows to swiftly follow the process from beginning to end with high accuracy and reliability as well as help in the design of a separation process.

2□ Materials and methods

2.1 Chemicals.

Lanthanum(III) nitrate hexahydrate $La(NO_3)_3{\cdot}6H_2O$ (purity 99.99 %), Neodymium(III) nitrate hexahydrate $Nd(NO_3)_3{\cdot}6H_2O$ (purity 99.99 %), Ytterbium(III) nitrate pentahydrate $Yb(NO_3)_3{\cdot}5H_2O$ (purity 99.99 %), Iron(III) nitrate nonahydrate $Fe(NO_3)_3{\cdot}9H_2O$ (purity 98 %), Nitric acid 70% and Citric Acid (purity 99 %) were purchased from Sigma Aldrich. The METALICAPT®-MFC-11 cation-exchange fiber with sulfonic acid (SO_3H) functional groups was purchased from AJELIS SAS.

2.2 Preparation of the initial solutions.

Initial standard solutions of sole La, Nd, Yb and Fe with an intended concentration of 250 mM each were respectively prepared by dissolving calculated and weighted amounts of $La(NO_3)_3{\cdot}6H_2O$, $Nd(NO_3)_3{\cdot}6H_2O$, $Yb(NO_3)_3{\cdot}5H_2O$ and $Fe(NO_3)_3{\cdot}9H_2O$ salts in a solution of nitric acid of different concentrations (0.1 M and 2M). Due to the hygroscopic nature of REEs nitrate salts, each of their solutions needed an initial calibration using ICP measurements to accurately determine their concentrations. All masses and final standard concentrations obtained via ICP are tabulated in the Supplementary Material (see Table S1). Finally, solution **A** was made by pipetting calculated volumes of each of these standard four solutions, in order to obtain a mixed solution in which each metal had a concentration of 30 mM.

A pure 3 M citric acid (Cit) solution was prepared by dissolving a calculated and weighted amount of solid citric acid in DI water (Milli-Q, 18.2 MΩ.cm at 25 °C). To study the impact of different Fe:Cit molar ratios on Fe adsorption, a calculated and pipetted volume of 3 M Cit was added to 55 mL of solution **A** (55 mL corresponded to the volume to be injected in the column during the adsorption step). Table S2 placed in the Supplementary Material presents the elemental concentrations calculated after the addition of the citric acid solution and the associated dilution.

2.3 Apparatus & accessories.

The millifluidic SPE platform is represented in **Fig. 1**. Its design was adapted from one dedicated to Liquid-Liquid extraction and previously reported [18]·[19]. It comprised of an extraction column with an embedded ion-exchange fiber where SPE occurs, a valve, and a downstream XRF optimized analytical chip, all mounted on a translational moving stage. This platform was fully integrated, and could quickly and efficiently perform the SPE process and the on-line XRF analysis of liquid output.

Analysis was performed using a homemade XRF spectrometer, which comprised of a static miniature X-ray tube equipped with a small XRF detector.

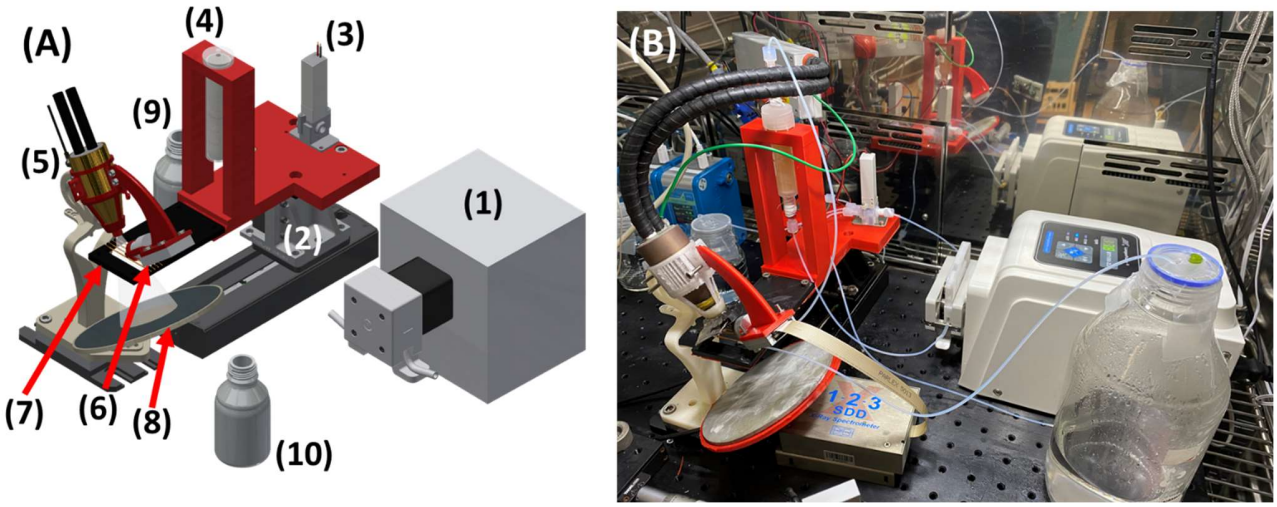

Fig. 1. (A) 3D view of the millifluidic platform. From right to left: peristaltic pump (1), motorized stage (2) holding one valve (3) and a chromatographic column (4) in which the fiber is wrapped, X-ray tube (5) placed inside its 3D-printed tube holder, XRF Detector (6) held by a 3D-printed arch screwed to the tube holder, and the XRF chip with a set of four Polyimide tubes

(7). A beam stop made of a circular tin plate (8) is located beneath the XRF chip. The glass reagent bottle in the background (9) contains the solution to be eluted in the column and the one in the forefront (10) is filled up with the output liquid (waste). (B) Real-life picture of the platform.

The extraction column was made up of Polypropylene (PP) with a total inner volume of 7.12 mL (see **Fig. 2A**) with the fiber based static phase already embedded, purchased from AJELIS SAS. All connections were made from Polyether Ether Ketone (PEEK) tubing purchased from Drawing-Microfluidics. The XRF chip comprised a set of four parallel sections of polyimide tubes (1.52 mm ID; 38 µm wall thickness) provided by Zeus Industrial Products, Inc. connected by PEEK tubes. Each connection was also reinforced with Polytetrafluoroethylene tape and finally glued with silicon seal purchased from RS Components and directly laid on a 3D-printed frame made to hold this set of tubing and the chip (see **Fig. 2B**).

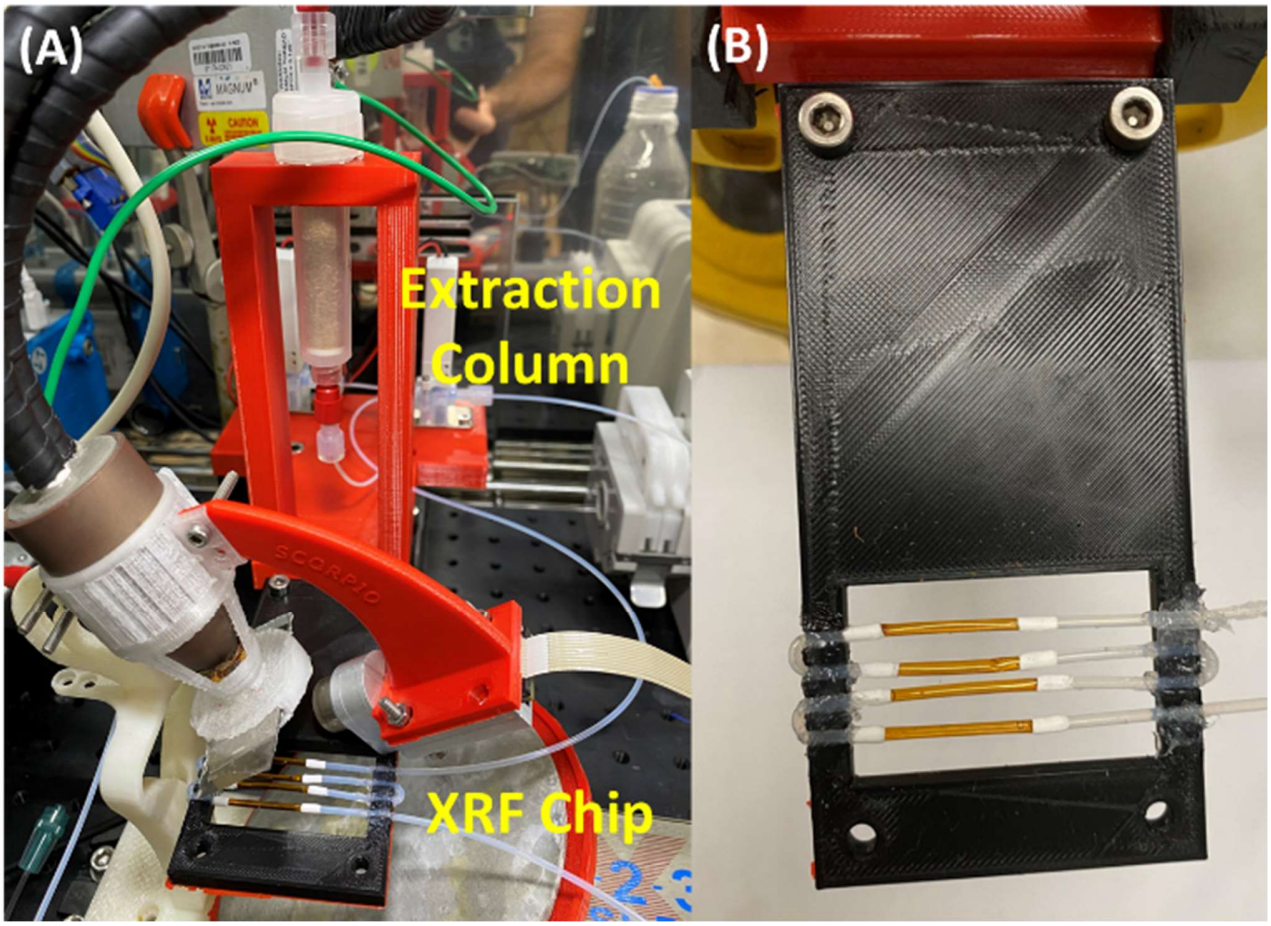

Fig. 2. (A) Close-up picture of the extraction column placed in its red 3D-printed holder and the XRF system. (B) XRF chip with its four Polyimide tubes glued onto a black 3D-printed holder frame.

The XRF spectrometer's hardware was composed of an X-ray source, an X-ray detector, and the assembly infrastructure. The X-ray tube was a Magnum 50 kV from Moxtek with a Silver anode. The X-ray detector was an X-123 SDD X-ray spectrometer from Amptek. The acquisition conditions were optimised to obtain the highest signal to noise (S/N) ratio when measuring Lanthanum, Neodymium, Ytterbium and Iron: 20 kV at 150 µA for the X-ray generator, an integration time of 120 s and a combination of two 50 µm-thick filters, one made of Titanium and the second of Silver. Both the calibration procedure and data treatment have been described previously by El Mangaar *et al.* [20] and Maurice *et al.* [18]. The quantities needed for the calibration procedure in the new geometry adopted for this work are recalled in the Supplementary Material (Table S3).

The entire platform was located within a Memmert, IPP 750 Plus temperature-controlled incubator, accurate to ± 0.1 °C. This also served as a safe X-ray enclosure, to enable its usage as per the required license provided by local authorities. Indeed, the chamber was wrapped with a 0.5 mm thick lead sheet, and all via holes were designed and shielded to fully protect users from ionizing radiations. A 5 mm circular tin plate stopped most of the X-ray beam after it had gone through the XRF chip. The fluidic tubing used to link the different parts were made of PEEK with an Internal Diameter (ID) of 0.45 mm and an Outside Diameter (OD) of 1.52 mm. For liquid injection, a peristaltic pump (BT100-2J) from The Longer Pump

Co., Ltd. with a DG-6 rollers pump head enabled a continuous flowrate. Specific Viton® tubing (1.6 mm ID x 2.4 OD) withstanding high acid concentrations was implemented in the pump head. The connections were made with PEEK fittings manufactured by Fluigent. The liquid valve was base mounted with 3-ports (2-way SMC LVM105R). To precisely put the Polyimide tubes embedded in the XRF chip at an optimized location according to the XRF detector and the X-ray beam, a Thorlabs motorized stage was used (DDSM100/M). All customized 3D parts were printed using an Ultimaker 3 Extended printer. The X-ray tube and the acquisition of spectra from the XRF detector were computer controlled using a homemade software programmed in Python 3+.

A pH-meter from Mettler-Toledo (S220) equipped with a pH probe was used to follow the pH of the adsorption solution.

3. RESULTS AND DISCUSSION

3.1 Millifluidic SPE.

One SPE experiment comprised of three main steps. The first step was the elution of the solution loaded with the metal ions concentrated at 30 mM. This step corresponded to the adsorption of the dissolved cations on the fiber. DI water was then eluted through the extraction column to avoid any contamination from any remaining initial solution in the column during the final step. Then, the metal elements previously captured by the fiber were fully desorbed using a highly concentrated HNO_3 solution (8.5 M). Indeed, preliminary tests showed that this acid concentration enabled a full regeneration of the fiber by removing all adsorbed metallic ions (see **Fig. S2** from the Supplementary Material). Furthermore, an ex-situ XRF analysis of a fiber which underwent a full extraction cycle, was performed using a handheld XRF from Olympus (Vanta C) and no remaining peak of the implemented metal elements was found. This analysis was done on three 250 mg fiber samples: one taken at the top, one in the centre and one at the bottom of the column.

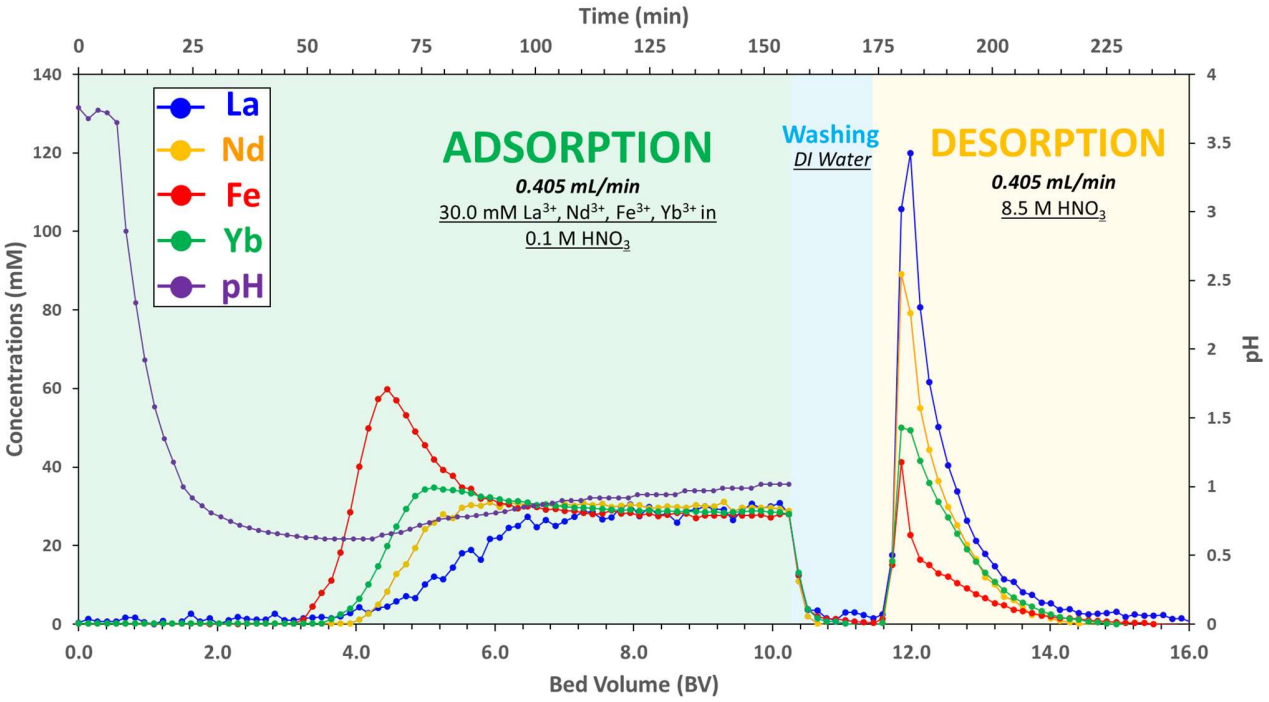

Fig. 3. SPE of La^{3+}, Nd^{3+}, Fe^{3+} and Yb^{3+} at 0.1 M HNO_3. Evolution of concentrations and pH as a function of bed volume (BV, mL) and time (min). NB: one bed volume of injected liquid corresponds to the total volume of the chromatographic column (7.12 mL)

All experiments were conducted at 25 °C. The liquid flowrate was chosen to allow us to observe the kinetics of both adsorption and desorption and was kept constant for these two steps.

Thanks to the integrated on-line XRF measurement, a full SPE process with periodic measurements (every 123 s) of all metals concentrations within the output solution took only 4 hours and 30 minutes and accounted for 100 mL. A usual measurement of the concentrations by ICP-OES would have more than doubled the total time for one extraction (taking into account the preparation of the solutions to be sent for ICP-OES, followed by their analysis) and would have resulted in nearly ten times more liquid waste.

Table 1. Experimental parameters for an SPE

Adsorption solution	30 mM La^{3+} 30 mM Nd^{3+} 30 mM Yb^{3+} 30 mM Fe^{3+} in 0.1 M HNO_3
Washing solution	DI water
Desorption solution	8.5 M HNO_3
Adsorption and Desorption flowrate	0.405 $mL.min^{-1}$
Temperature	25.0 °C

Finally, as an acidic cation exchange fiber was implemented in this study, a pH measurement of the output liquid during the adsorption step was also conducted. Indeed, H^+ protons are released when exchanged with metal ions and can serve as a tracer of the stationary phase exchange capacity.

3.2 REEs and Fe SPE.

Firstly, an SPE involving an adsorption solution of 30 mM of La(III), Nd(III), Fe(III) and Yb(III) in 0.1 M HNO_3 was implemented in order to get an idea of how the adsorption process was behaving between these four metal elements and H^+. **Table 1** summarises the experimental parameters for the SPE presented here. The graph presented **Fig. 3** shows the evolution of the metal ion concentrations, followed by on-line XRF during the three process steps, and the pH during the adsorption step. This first SPE experiment was cycled four times to check the result repeatability and see if there was any modification undergone by the fiber. It showed similar adsorption and desorption curves for each of the four cycles (see Supplementary Material **Fig. S3**).

At the beginning of the elution of the REEs plus Fe mixture, the pH slowly decreased from 4, as the fiber was initially washed with DI water, until it reached its lowest value of 0.62 for a BV = 3.7 ± 0.2. H^+ is therefore the very first ionic species piercing out of the column, as the metal concentrations had not increased. This decrease in the pH value was due to the cationic exchange taking place on the fiber, where H^+ protons were replaced by metallic ions: the fiber was being loaded with the REEs and iron. Before pH reached its minimum, Fe(III) was the first metal element to see its concentration curve increasing at BV = 3.3 ± 0.1. This means that iron had reached its loading capacity and therefore pierces out of the column. From BV equal to 4.4 ± 0.1 to 10.2 ± 0.1 (end of adsorption), pH was then slowly increased towards pH equal to 1, which corresponds to the pH value of the input adsorption solution concentrated at 0.1 M in HNO_3. One then measured the piercing of Yb(III), Nd(III) and finally La(III) at BV equal to 3.7 ± 0.1, 4.1 ± 0.2 and 3.8 ± 1.0, respectively. One should note that the BV standard deviation of Lanthanum is the highest because of a low S/N ratio for La's XRF peaks at low concentrations. As metal elements' concentrations were plateauing starting at 7.5 BV, pH was still levelling off to its plateau at 1, resulting in a selectivity competition between these five species, namely La(III), Nd(III), Fe(III), Yb(III) and H^+. Many SPE studies report the influence of the pH of the initial adsorption solution on the extraction efficiency, where they specifically mention this competition between metal ions and protons [21–26]. However, beyond varying the pH of the initial solution to be eluted, following the pH during the adsorption allowed us to get a better understanding of this protonic competition [27]. In addition, extraction processes involving either a weakly acidic fiber or a strongly acidic one (with all the other experimental parameters fixed) would lead to different extraction efficiencies [28]. Indeed, the interactions between a binding site on the fiber and a proton will differ because of their different acidic constants, resulting in final different selectivity competitions between all the involved species.

At the end of the adsorption step, the output metal concentration was measured as equal to the input concentration (30 mM) indicating that all adsorption sites of the cation-exchange fiber were occupied: the fiber was saturated and no more interaction between the eluting liquid and the fiber occurred. After the washing step with DI to rinse out the adsorption solution, the desorption step showed four peaks, one for each element. The highest peak refers to La(III) and, as the area under the desorption curve is proportional to the molar quantity of the adsorbed species on the fiber, La(III) was consequently the most adsorbed element, compared to the others. Indeed, lower peak maxima were measured for La(III), Nd(III) both around 95 mM, Yb(III) at 50 mM and finally Fe(III) at a little more than 40 mM.

The fact that Fe(III) had the smallest desorption peak can be related to the 60 mM peak maximum for Fe(III) concentration at 4.5 BV during the adsorption step. Indeed, such a peak can be explained as coming from the competition between each element versus the binding site on the fiber [29]. Calculations, placed in the Supplementary Material (see **Section 6.**), show that the amount of adsorbed iron is effectively equivalent to the total desorbed Fe(III) during both the adsorption peak at 4.5 BV and the desorption peak. Therefore, we can conclude from the observation of this 4.5 BV iron peak that some Fe(III)

desorption is induced by its lower affinity with the fiber when compared to La(III), Nd(III) and Yb(III). To a lesser extent, this is also observed for Yb(III), with a broad peak centred at ~5 BV.

The desorption curves also enable a determination of the total exchange capacity, or retention capacity, of the fiber allowing a comparison with the commercial value given by the manufacturer (3-6 eq/kg_{fiber}). The calculation of this exchange capacity is determined for each species and then summed in order to get the total capacity. The retention capacity is given by **Equation 1** as follows:

$$c_{retention,i} = \frac{eq_i}{m_{fibre}} \qquad (1)$$

Where eq_i (mol) is the molar equivalent, which refers to the molar quantity of adsorbed species I on the fiber, determined by the product of the area under the desorption curve for element I by the cationic charge (+3 for every element included in this study) and m_{fiber} (kg_{fiber}) is the mass of the fiber wrapped in the column.

Table 2. Exchange capacities of REEs and Fe and total capacity of the cation-exchange fiber

Element	Retention capacity $c_{retention}$ (eq/kg_{fiber})
La	0.72 ± 0.04
Nd	0.51 ± 0.03
Yb	0.22 ± 0.02
Fe	0.41 ± 0.02
Total capacity	1.87 ± 0.11

Table 2 gives the retention capacities for La(III), Nd(III), Yb(III) and Fe(III). Supplementary Material **Fig. S5** depicts the area under each element's curve used for the determination of their respective retention capacity.

Overall, the total retention capacity of the fiber is of the same order of magnitude, although slightly smaller than the value of 3-6 eq/kg_{fiber} given by the manufacturer. This is due to the low pH at which we were working, which favours the protonation of the binding sites instead of the exchange of a proton by a cation.

3.3 Adsorption: Experimental data modelling.

The performance of a fixed-bed column assessed experimentally can be compared with adsorption mechanisms theoretical performance. Usually, only the curve obtained during the adsorption step, called the breakthrough curve, is modelled and evaluated with the implemented experimental parameters (flowrate, bed height, initial concentration).

Throughout this SPE study, several theoretical models were tested (Adams-Bohart [30], Li [31], Thomas [32], Yoon-Nelson [33]). Among these models, only two are presented in this report as they show the closest fit with our experimental data. The first one is the Thomas model, which is the most widely used mathematical model in the prediction of breakthrough curves. This model is based on a Langmuir equilibrium, second-order reversible kinetics and a plug-flow-based flow system. External and internal diffusion resistances are ignored in this model. The Thomas model is expressed by **Equation 2**.

$$\frac{C_i}{C_0} = \frac{1}{1+\exp\left(\frac{k_{T,i}q_{T,i}m_{fibre}}{Q} - k_{T,i}C_0 t\right)} \qquad (2)$$

Where C_i and C_o (g/L) are the concentrations of the species i at time t and t_o, respectively, $k_{T,i}$ (mL.min^{-1}.g^{-1}) is the Thomas rate constant of the species i, $q_{T,i}$ (mg/g) is the adsorption capacity of the fiber of the species i, m_{fiber} (g) is the mass of the fiber wrapped in the column, Q (mL/min) is the liquid flowrate and t (min) the time.

The second implemented model is the Yoon-Nelson model, which is based on the adsorption theory and breakthrough of adsorbate probability. This model is described by **Equation 3** :

$$\frac{C_i}{C_0} = 1 - \frac{1}{1+\left(\frac{C_0 Q t}{q_{YN,i}m_{fibre}}\right)^{a_i}} \qquad (3)$$

Where C_i and C_o (g/L) are respectively the concentration of the species i at time t and t_o. Q (mL/min) is the liquid flowrate, t (min) the time, $q_{YN,i}$ (mg/g) is the adsorption capacity of the fiber of the species i, m_{fiber} (g) is the mass of the fiber wrapped in the column and a_i is an empirical parameter determined experimentally of the species i.

Linear regressions of these two models were performed in order to determine the parameters k_T and q_T for the Thomas model and a and q_{YN} for the Yoon-Nelson model. Besides, only the experimental data of Lanthanum and Neodymium were used, because Iron and Ytterbium display a desorption peak during their respective breakthrough curve. **Table 3** gives the values of the Thomas and Yoon-Nelson parameters as well as their corresponding R-squared value.

Table 3. Thomas and Yoon-Nelson models' parameters

Element	Thomas Model			Yoon-Nelson Model		
	k_T ($mL.min^{-1}.g^{-1}$)	q_T (mg/g)	r^2	a	q_{YN} (mg/g)	r^2
La	0.010	63	0.95	7.8	8.9	0.93
Nd	0.97	0.03	57	21	8.5	0.98

After the determination of these values, simulated breakthrough curves for both Lanthanum and Neodymium were plotted (see Fig. 4 (a) and (b)). On each graph, the experimental concentration of the species, the Thomas model concentration and finally, the Yoon-Nelson model concentration were plotted. One should note that the x-axis of each graph starts at the time of the experiment when the corresponding element is piercing (defined as 1% of the initial concentration).

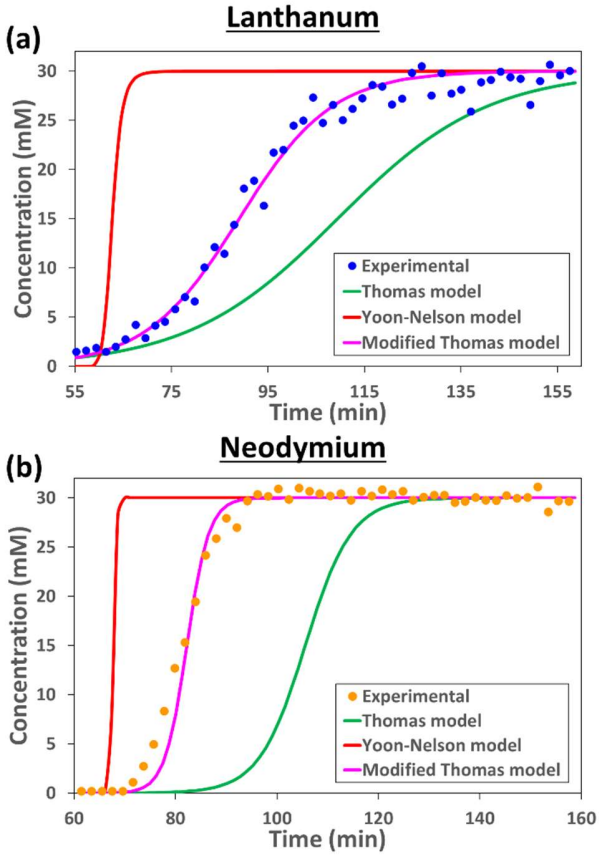

Fig. 4. Thomas (green), Yoon-Nelson (red) and modified Thomas (pink) models compared to experimental data for Lanthanum (a) and Neodymium (b).

However, neither model led to a good fit of the experimental data. We interpreted this as due to the use of a multi-component extraction system. Indeed, if some reports showed a good accuracy of the Thomas model when dealing with extractions of multiple ions [34,35], a majority of studies also pointed out unfitting data in such multi-species cases for the Thomas model[36–39]. A new Thomas model was even proposed by Yan *et al.* [38] and confirmed [39], that still could not fit our data. Hence, a phenomenological approach was considered by adding a corrective coefficient to the two models. While this

attempt failed for the Yoon-nelson model, a theoretical adjusted Thomas model was found to fit our experimentally obtained breakthrough curves. **Equation 4** gives the updated equation from the initial Thomas model.

$$\frac{C_i}{C_0} = \frac{1}{1+\exp(\frac{k_{T,i}q_{T,i}m_{fibre}}{Q} - \alpha_i k_{T,i} C_0 t)} \qquad (4)$$

Where α_{La} = 1.6 and α_{Nd} = 2.1.

In **Equation 4**, an apparent rate constant under the expression $k_{app,i} = \alpha_i k_{T,i}$ (i = La or Nd) reflects a new rate constant for this adapted Thomas model. The fit for this model for both Lanthanum and Neodymium was also plotted, see **Fig. 4** (a) and (b), respectively. To further test the applicability of this modified model, an SPE involving a single REE (Nd) was performed, and the data fit well with the proposed modified Thomas model (see **Fig. S6** in the Supplementary Material). The alpha value for this single ion extraction was adjusted at α_{Nd} = 2.6, which differs from the one obtained for the multi-ion extraction, α_{Nd} = 2.1. Therefore, the modified Thomas model presented herein does not only stem from the implementation of a multi-ion extraction system, it also derives from the fact that we are using synthetic fibres with a far higher exchange surface area than conventional ion-exchange resin [40–45]. Moreover, Liu et al. also reported that an unsmooth interface such as our fiber materials may have an effect on the existing predicted models [46]. With such fibers, cation diffusion to the binding site plays little role, hence allowing for faster sorption kinetics. This could explain why such kinetic observations have seldom been reported, as well as the need to adjust the theoretical modelling as shown by Vuorio et al. [41].

3.4 Selective separation of Fe(III).

Inspired by the previous multi-components results, highlighting the two different behaviors between Fe(III) and the other REEs, we investigated a potentially new separation process via selective extraction. Its aim was to remove or reduce as much as possible the concentration of Fe(III) in the desorption stream. An organic acid was chosen that would modify the overall charge of the involved cation complexes (the ion speciation), resulting in a difference of interaction with the cation-exchange fiber. Based on our literature search, we chose Citric Acid, which is a well-known complexing agent, particularly towards Fe(II) and Fe(III) [47–49]. This choice was further confirmed by simulation using Hydra-Medusa software, which allowed us to predict: (i) the formation of the complex $[FeHCit]^+$, between Citrate (Cit: $C6H_5O_7^{3-}$), Fe^{3+} and H^+ and; (ii) that Lanthanum, Neodymium and Ytterbium are not coordinated by Cit in low pH solutions. Fe:Cit molar ratios were first experimentally optimized prior to studying the role of HNO_3 concentrations. The amount of desorbed Fe(III) was determined by varying the Fe:Cit = 1:X molar ratios (where X = 1, 2, 4, 6, 10 and 20). The results obtained, and displayed in Fig. 5, indicate that the molar quantity of desorbed Fe(III) decreases when the Fe:Cit molar ratio increases. Hence, in order to get the least absorption of Fe(III) on the fiber, a Fe:Cit molar ratio of 1:20 and a 0.1 M HNO_3 were determined to be best. An SPE implementing these specific experimental parameters (Fe:Cit = 1:20 and 0.1 M HNO_3) was performed and followed by on-line XRF and furthermore confirmed by ICP-OES measurements. Overall, the latter off-line analysis tripled the amount of time required to performed the analysis (12h 30min) and produced more than 8 time the amount of waste (830 mL) when compared to what can be achieved when using purely the on-line XRF tool. The graph presenting the evolution of the concentrations during the extraction process with the implementation of the optimized parameters (within the range of our study) can be found Fig. 6 (XRF (a) and ICP-OES (b)). The two trends remain the same between XRF and ICP followed extractions. However, one can note that the concentration scale differs. Indeed, for the ICP-followed extraction, 1 mL of output solution was collected every 2.78 mins, while for the XRF-followed extraction, one spectrum acquisition lasted 2.05 min. For the ICP

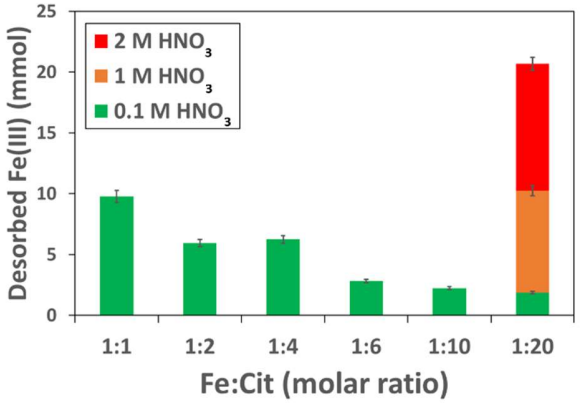

Fig. 1. Molar quantity (mmol) of desorbed Fe^{3+} for different Fe:Cit molar ratios and HNO_3 concentrations.

method, concentrations' samples are reflected as averaged within 1 mL volume sample, whereas for the XRF method, a continual flow with concentrations' gradients is measured. Consequently, concentrations displayed on the Y-axis cannot be compared together.

Results show that if one is willing to recover REEs with some traces of Fe, sampling virtually all the desorption eluant is of interest. Also, pure Fe can be obtained at the beginning of the adsorption step, which can be followed by the recovery of a small amount of a Fe-Yb mixture.

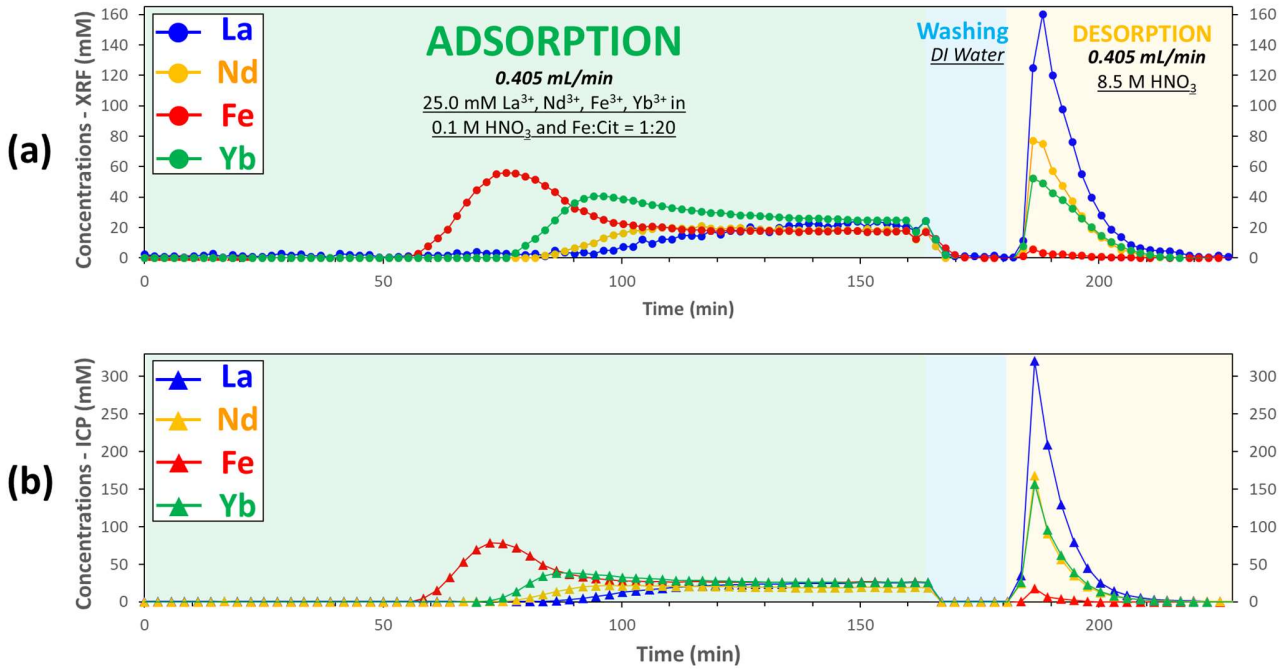

Fig. 6. SPE of La^{3+}, Nd^{3+}, Fe^{3+} and Yb^{3+} at 0.1 M HNO_3 and Fe:Cit = 1:20. Evolution of concentrations followed by XRF (a) and ICP-OES (b) as a function of time.

4. CONCLUSION

The millifluidic platform presented in this report showed that it can enable a fast and accurate implementation of S-P metal extraction processes. The downstream on-line XRF analysis of the output solution helps to reduce the analysis time down to a few hours and reduces liquid waste. Thus, we have proved that this platform is capable of completing a whole SPE study from the choice of the solid-phase to the concentrations of the solutions to be eluted. Indeed, once the chemical system has been determined, the analysis parameters have been fine-tuned, and the XRF calibration routine has been performed, the platform is ready to run a comprehensive chemical engineering-related study. Furthermore, a modified phenomenological adsorption model based on the theoretical Thomas model has also been proposed that fits well with experimental data.

From this multi-component system, a speciation-based separation could be derived where the use of an organic acid at a specific molar ratio avoided significant adsorption of iron on the fiber, leading to a final desorbed solution virtually free of iron. This would embody a first important step when dealing with streams loaded with REEs and Fe, particularly when recovering Nd from NdFeB magnets.

Furthermore , we have also shown that we could use this platform to find an optimal operating point by rapidly and efficiently screening ranges of different experimental parameters. This kind of setup could particularly help building an ion-exchange simulation bed with fast determination of operating points of a given SPE process [50].

Finally, thanks to the selectivity and sensitivity of the XRF spectrometry, a very wide range of different metal mixtures can be studied using this platform, as long as element studied have an atomic number greater than 22 (Titanium), that their XRF peaks do not overlap and that their concentrations are above 1 $mmol.L^{-1}$. This platform should therefore definitely be of interest for most industry wanting to implement such processes on a larger scale.

ASSOCIATED CONTENT

Supplementary Material

Calibration procedure, data and curves for the XRF measurement. Additional experimental results with lower importance. (PDF)

AUTHOR INFORMATION

Corresponding Author

* E-mail: jean-christophe.gabriel@cea.fr (J.-C.P.G.)

Author Contributions

JCG conceptualized the study; FO adapted the integrated platform into millifluidics; JCG and FO defined the methodology; BK performed preliminary studies using offline ICP; FO assembled the XRF integrated millifluidic platform and performed millifluidic experimental investigations, data collection and data curation; and with JCG and SC their interpretation; FO and JCG wrote first draft; All authors contributed to further writing, review & editing of the article; JCG managed, coordinated and supervised as well as secured fundings.

Declaration of Competing Interest

The authors declare no competing interests.

Acknowledgments

FO, SC and J.C.G. acknowledge financial support from SCARCE project, which is supported by the National Research Foundation, Singapore, and National Environment Agency, Singapore under its Closing the Waste Loop Funding Initiative (Award No. USS-IF-2018-4). J.C.G. acknowledges funding for the platform from the European Research Council under the European Union's 7th Framework Program (FP/2007-2013)/ERC Grant Agreement N° [320915] "REE-CYCLE": Rare Earth Element reCYCling with Low harmful Emissions. BK acknowledges financial support from the European Research Council under the European Union's 7th Framework Program (FP/2007-2013)/ERC Proof of Concept Grant Agreement N° [768722] "SYNEXTRACT": All Aqueous, continuous, Solid-Liquid SYNergistic EXTRACTion of rare earth elements. FO thanks CEA's program "Matériaux et Procédés" for a PhD grant support (project MICROPRO).

FO acknowledges discussions with AJELIS's CEO, Dr. Ekatarina Shilova, regarding AJELIS past experience with the selective separation of multicomponent critical metal solutions by elution with acids or complexing reagents of different concentrations using METALICAPT®.

We are indebted to Thomas Zemb and Daniel Meyer for useful scientific discussions and for manuscript critical reading and suggestions.

References

[1] D. Vuckovic, E. Cudjoe, F.M. Musteata, J. Pawliszyn, Automated solid-phase microextraction and thin-film microextraction for high-throughput analysis of biological fluids and ligand-receptor binding studies, Nat. Protoc. 5 (2010) 140–161. https://doi.org/10.1038/nprot.2009.180.

[2] X. Zhang, K.D. Oakes, D. Luong, C.D. Metcalfe, M.R. Servos, Solid-phase microextraction coupled to LC-ESI-MS/MS: Evaluation and correction for matrix-induced ionization suppression/enhancement for pharmaceutical analysis in biological and environmental samples, Anal. Chem. 83 (2011) 6532–6538. https://doi.org/10.1021/ac200718d.

[3] X. Zhang, K.D. Oakes, M.E. Hoque, D. Luong, S. Taheri-Nia, C. Lee, B.M. Smith, C.D. Metcalfe, S. De Solla, M.R. Servos, Depth-profiling of environmental pharmaceuticals in biological tissue by solid-phase microextraction, Anal. Chem. 84 (2012) 6956–6962. https://doi.org/10.1021/ac3004659.

[4] E. Simeonov, I. Seikova, I. Pentchev, A. Mintchev, Scale-up of the solid-liquid extraction using characteristic function technique, Ind. Eng. Chem. Res. 43 (2004) 4903–4907. https://doi.org/10.1021/ie030650m.

[5] R. Sasai, N. Shimamura, T. Fujimura, Eco-Friendly Rare-Earth-Metal Recovering Process with High Versatility from Nd-Fe-B Magnets, ACS Sustain. Chem. Eng. 8 (2020) 1507–1512. https://doi.org/10.1021/acssuschemeng.9b05996.

[6] D. Prodius, K. Gandha, A.V. Mudring, I.C. Nlebedim, Sustainable Urban Mining of Critical Elements from Magnet and Electronic Wastes, ACS Sustain. Chem. Eng. 8 (2020) 1455–1463. https://doi.org/10.1021/acssuschemeng.9b05741.

[7] Y. Bian, S. Guo, L. Jiang, J. Liu, K. Tang, W. Ding, Recovery of Rare Earth Elements from NdFeB Magnet by VIM-HMS Method, ACS Sustain. Chem. Eng. 4 (2016) 810–818. https://doi.org/10.1021/acssuschemeng.5b00852.

[8] N.A. Chowdhury, S. Deng, H. Jin, D. Prodius, J.W. Sutherland, I.C. Nlebedim, Sustainable Recycling of Rare-Earth Elements from NdFeB Magnet Swarf: Techno-Economic and Environmental Perspectives, ACS Sustain. Chem. Eng. 9 (2021) 15915–15924. https://doi.org/10.1021/acssuschemeng.1c05965.

[9] S.K. Haider, S.K. Haider, S.K. Haider, J.Y. Lee, D. Kim, D. Kim, Y.S. Kang, Eco-Friendly Facile Three-Step Recycling Method of (Nd-RE)2Fe14B Magnet Sludge and Enhancement of (BH)maxby Ball Milling in Ethanol, ACS Sustain. Chem. Eng. 8 (2020) 8156–8163. https://doi.org/10.1021/acssuschemeng.0c00584.

[10] Z. Liu, J. Wu, X. Liu, W. Wang, Z. Li, R. Xu, Y. Ding, J. Wang, Recovery of neodymium, dysprosium, and cobalt from NdFeB magnet leachate using an unsymmetrical dialkylphosphinic acid extractant, INET-3, J. Rare Earths. 38 (2020) 1114–1118. https://doi.org/10.1016/j.jre.2020.01.018.

[11] B. Liu, N. Zhu, Y. Li, P. Wu, Z. Dang, Y. Ke, Efficient recovery of rare earth elements from discarded NdFeB magnets, Process Saf. Environ. Prot. 124 (2019) 317–325. https://doi.org/10.1016/j.psep.2019.01.026.

[12] B. Dewulf, N.K. Batchu, K. Binnemans, Enhanced Separation of Neodymium and Dysprosium by Nonaqueous Solvent Extraction from a

Polyethylene Glycol 200 Phase Using the Neutral Extractant Cyanex 923, ACS Sustain. Chem. Eng. 8 (2020) 19032–19039. https://doi.org/10.1021/acssuschemeng.0c07207.
[13] D. Xia, N.M. Charpentier, A.A. Maurice, A. Brambilla, Q. Yan, J.-C.P. Gabriel, Sustainable route for Nd recycling from waste electronic components featured with unique element-specific sorting enabling simplified hydrometallurgy, Chem. Eng. J. 441 (2022) 135886. https://doi.org/10.1016/j.cej.2022.135886.
[14] A. Sun, Q. Xu, L. Ren, G. Cao, D. Gou, Non-equilibrium ultrasound-assisted solid-liquid extraction of boron present in different phases within plants by ICP-OES, RSC Adv. 7 (2017) 49890–49894. https://doi.org/10.1039/c7ra07078k.
[15] A. Saha, K. Sanyal, N. Rawat, S.B. Deb, M.K. Saxena, B.S. Tomar, Selective Micellar Extraction of Ultratrace Levels of Uranium in Aqueous Samples by Task Specific Ionic Liquid Followed by Its Detection Employing Total Reflection X-ray Fluorescence Spectrometry, Anal. Chem. 89 (2017) 10422–10430. https://doi.org/10.1021/acs.analchem.7b02427.
[16] A.M. McKenna, H. Chen, C.R. Weisbrod, G.T. Blakney, Molecular comparison of solid-phase extraction and liquid/liquid extraction of water-soluble petroleum compounds produced through photodegradation and biodegradation by ft-icr mass spectrometry, Anal. Chem. 93 (2021) 4611–4618. https://doi.org/10.1021/acs.analchem.0c05230.
[17] A.A. Cuthbertson, C. Bach, S.D. Richardson, X. Dauchy, A novel automated method for the quantification of ten halobenzoquinones in drinking water using online solid-phase extraction coupled with liquid chromatography tandem mass spectrometry, J. Chromatogr. A. 1612 (2020) 460642. https://doi.org/10.1016/j.chroma.2019.460642.
[18] A.A. Maurice, J. Theisen, V. Rai, F. Olivier, A. El Maangar, J. Duhamet, T. Zemb, J.C.P. Gabriel, First online X-ray fluorescence characterization of liquid-liquid extraction in microfluidics, Nano Sel. (2021) 1–12. https://doi.org/10.1002/nano.202100133.
[19] F. Olivier, A.A. Maurice, J.C.P. Gabriel, Liquid-liquid extraction : thermodynamics-kinetics driven processes explored by microfluidics, Compte-Rendus l'Académie Des Sci. - Chim. (2022).
[20] A. El Maangar, J. Theisen, C. Penisson, T. Zemb, J.C.P. Gabriel, A microfluidic study of synergic liquid-liquid extraction of rare earth elements, Phys. Chem. Chem. Phys. 22 (2020) 5449–5462. https://doi.org/10.1039/c9cp06569e.
[21] A. Saeed, M. Iqbal, M.W. Akhtar, Removal and recovery of lead(II) from single and multimetal (Cd, Cu, Ni, Zn) solutions by crop milling waste (black gram husk), J. Hazard. Mater. 117 (2005) 65–73. https://doi.org/10.1016/j.jhazmat.2004.09.008.
[22] W.W. Sułkowski, K. Nowak, A. Sułkowska, B. Mikuła, P. Wierzba, The conditions of cationic exchange with the use of recycling polystyrene derivative, the product of sulfonation by silica sulfuric acid, J. Appl. Polym. Sci. 128 (2013) 2611–2617. https://doi.org/10.1002/app.38429.
[23] H. Farrah, D. Hatton, W.F. Pickering, The affinity of metal ions for clay surfaces, Chem. Geol. 28 (1980) 55–68. https://doi.org/10.1016/0009-2541(80)90035-2.
[24] S.K. Papageorgiou, F.K. Katsaros, E.P. Kouvelos, J.W. Nolan, H. Le Deit, N.K. Kanellopoulos, Heavy Metal Sorption By Calcium Alginate Beads From Laminaria Digitata, J. Hazard. Mater. (2006) 1765–1772. https://doi.org/10.1016/j.jhazmat.2006.05.017.
[25] C.J. Milne, D.G. Kinniburgh, J.C.M. de Wit, W.H. van Riemsdijk, L.K. Koopal, Analysis of metal-ion binding by a peat humic acid using a simple electrostatic model, J. Colloid Interface Sci. 175 (1995) 448–460. https://doi.org/10.1006/jcis.1995.1475.
[26] K.S. Low, C.K. Lee, K.P. Lee, Sorption of copper by dye-treated oil-palm fibres, Bioresour. Technol. 44 (1993) 109–112. https://doi.org/10.1016/0960-8524(93)90183-C.
[27] J. Griffioen, Multicomponent cation exchange including alkalinization/acidification following flow through sandy sediment, Water Resour. Res. 29 (1993) 3005–3019. https://doi.org/10.1029/93WR01067.
[28] F.G. Helfferich, Ion Exchange: Past, Present, and Future BT - Ion Exchange: Science and Technology, in: A.E. Rodrigues (Ed.), Springer Netherlands, Dordrecht, 1986: pp. 23–32. https://doi.org/10.1007/978-94-009-4376-6_2.
[29] F. Evangelista, F.C. Di Berardino, Modelling of Multicomponent Fixed Bed Ion Exchange Operations BT - Ion Exchange: Science and Technology, in: A.E. Rodrigues (Ed.), Springer Netherlands, Dordrecht, 1986: pp. 255–269. https://doi.org/10.1007/978-94-009-4376-6_9.
[30] G.S. Bohart, E.Q. Adams, Some aspects of the behavior of charcoal with respect to chlorine, J. Am. Chem. Soc. 42 (1920) 523–544. https://doi.org/10.1021/ja01448a018.
[31] Y. Liu, C. Wang, S. Li, A Fractal Langmuir Kinetic Equation And Its Solution Structure, Therm. Sci. (2021) 2–5. https://doi.org/10.2298/TSCI200320033L.
[32] H.C. Thomas, Heterogeneous Ion Exchange in a Flowing System, J. Am. Chem. Soc. 66 (1944) 1664–1666. https://doi.org/10.1021/ja01238a017.
[33] Y.H. Yoon, J.H. Nelson, Application of Gas Adsorption Kinetics I. A Theoretical Model for Respirator Cartridge Service Life, Am. Ind. Hyg. Assoc. J. 45 (1984) 509–516. https://doi.org/10.1080/15298668491400197.
[34] X. You, A. Farran, D. Guaya, C. Valderrama, V. Soldatov, J.L. Cortina, Phosphate removal from aqueous solutions using a hybrid fibrous exchanger containing hydrated ferric oxide nanoparticles, J. Environ. Chem. Eng. 4 (2016) 388–397. https://doi.org/10.1016/j.jece.2015.11.032.
[35] D.Q. Melo, C.B. Vidal, A.L. Da Silva, R.N.P. Teixeira, G.S.C. Raulino, T.C. Medeiros, P.B.A. Fechine, S.E. Mazzeto, D. De Keukeleire, R.F. Nascimento, Removal of Cd2+, Cu2+, Ni2+, and Pb 2+ ions from aqueous solutions using tururi fibers as an adsorbent, J. Appl. Polym. Sci. 131 (2014) 1–12. https://doi.org/10.1002/app.40883.
[36] M.M. Bello, M.M. Nourouzi, L.C. Abdullah, T.S.Y. Choong, Y.S. Koay, S. Keshani, POME is treated for removal of color from biologically treated POME in fixed bed column: Applying wavelet neural network (WNN), J. Hazard. Mater. 262 (2013) 106–113. https://doi.org/10.1016/j.jhazmat.2013.06.053.
[37] S.J. Kleinübing, E. Guibal, E.A. da Silva, M.G.C. da Silva, Copper and nickel competitive biosorption simulation from single and binary systems by Sargassum filipendula, Chem. Eng. J. 184 (2012) 16–22. https://doi.org/10.1016/j.cej.2011.11.023.
[38] G. Yan, T. Viraraghavan, M. Chen, A new model for heavy metal removal in a biosorption column, Adsorpt. Sci. Technol. 19 (2001) 25–43. https://doi.org/10.1260/0263617011493953.
[39] L.F. Lima, J.R. De Andrade, M.G.C. Da Silva, M.G.A. Vieira, Fixed Bed Adsorption of Benzene, Toluene, and Xylene (BTX) Contaminants from Monocomponent and Multicomponent Solutions Using a Commercial Organoclay, Ind. Eng. Chem. Res. 56 (2017) 6326–6336. https://doi.org/10.1021/acs.iecr.7b00173.
[40] L. Chen, G. Yang, J. Zhang, A study on the exchange kinetics of ion-exchange fiber, React. Funct. Polym. 29 (1996) 139–144. https://doi.org/10.1016/1381-5148(95)00070-4.
[41] M. Vuorio, J.A. Manzanares, L. Murtomäki, J. Hirvonen, T. Kankkunen, K. Kontturi, Ion-exchange fibers and drugs: A transient study, J. Control. Release. 91 (2003) 439–448. https://doi.org/10.1016/S0168-3659(03)00270-0.
[42] E. Kamio, K. Kondo, Separation of rare metal ions by a column packed with microcapsules containing an extractant, Ind. Eng. Chem. Res. 41 (2002) 3669–3675. https://doi.org/10.1021/ie010737c.
[43] S. Bao, Y. Tang, Y. Zhang, L. Liang, Recovery and Separation of Metal Ions from Aqueous Solutions by Solvent-Impregnated Resins, Chem.

Eng. Technol. 39 (2016) 1377–1392. https://doi.org/10.1002/ceat.201500324.
[44] E. Kamio, Y. Fujiwara, M. Matsumoto, F. Valenzuela, K. Kondo, Investigation on extraction rate of lanthanides with extractant-impregnated microcapsule, Chem. Eng. J. 139 (2008) 93–105. https://doi.org/10.1016/j.cej.2007.07.072.
[45] S. Lacour, J.C. Bollinger, B. Serpaud, P. Chantron, R. Arcos, Removal of heavy metals in industrial wastewaters by ion-exchanger grafted textiles, Anal. Chim. Acta. 428 (2001) 121–132. https://doi.org/10.1016/S0003-2670(00)01215-0.
[46] X. Li, Z. Liu, J.H. He, A Fractal Two-Phase Flow Model for the Fiber Motion in a Polymer Filling Process, Fractals. 28 (2020) 1–10. https://doi.org/10.1142/S0218348X20500930.
[47] R.E. Hamm, C.M. Shull, D.M. Grant, Citrate Complexes with Iron (II) and Iron (III), J. Am. Chem. Soc. 76 (1954) 2111–2114. https://doi.org/10.1021/ja01637a021.
[48] A.M.N. Silva, X. Kong, M.C. Parkin, R. Cammack, R.C. Hider, Iron(iii) citrate speciation in aqueous solution, Dalt. Trans. (2009) 8616–8625. https://doi.org/10.1039/b910970f.
[49] X. Feng, Z. Wang, Y. Chen, T. Tao, F. Wu, Y. Zuo, Effect of Fe(III)/citrate concentrations and ratio on the photoproduction of hydroxyl radicals: Application on the degradation of diphenhydramine, Ind. Eng. Chem. Res. 51 (2012) 7007–7012. https://doi.org/10.1021/ie300360p.
[50] A.E. Rodrigues, Ion exchange in agitated beds, J. Chromatogr. A. 102 (1974) 437–442. https://doi.org/10.1016/s0021-9673(01)85477-7.